

# The micro-distribution of carbonaceous matter in the Murchison meteorite as investigated by Raman imaging

Chahrazade El Amri<sup>a</sup>, Marie-Christine Maurel<sup>b</sup>, Gérard Sagon<sup>c</sup>, Marie-Hélène Baron<sup>c,\*</sup>

<sup>a</sup> *Laboratoire de Bioactivation des Peptides, Institut Jacques-Monod, Université Paris VI, tour 43, 2, place Jussieu, Paris Cedex 75251, France*

<sup>b</sup> *Laboratoire de Biochimie de l'Evolution et Adaptabilité Moléculaire, Institut Jacques-Monod, Université Paris VI, tour 43, 2, place Jussieu, Paris Cedex 75251, France*

<sup>c</sup> *Laboratoire de Dynamique Interactions et Réactivité, CNRS-UMR 7075, Université Paris VI, 2, rue Henri Dunant, Thiais 94320, France*

Received 18 March 2004; accepted 2 August 2004

## Abstract

The carbonaceous Murchison chondrite is one of the most studied meteorites. It is considered to be an astrobiology standard for detection of extraterrestrial organic matter. Considerable work has been done to resolve the elemental composition of this meteorite. Raman spectroscopy is a very suitable technique for non-destructive rapid in situ analyses to establish the spatial distribution of carbonaceous matter. This report demonstrates that Raman cartography at a resolution of  $1\ \mu\text{m}^2$  can be performed. Two-dimensional distribution of graphitised carbon, amorphous carbonaceous matter and minerals were obtained on  $100\ \mu\text{m}^2$  maps. Maps of the surface of native stones and of a powdered sample are compared. Graphitic and amorphous carbonaceous domains are found to be highly overlapping in all tested areas at the surface of the meteorite and in its interior as well. Pyroxene, olivine and iron oxide grains are embedded into this mixed carbonaceous material. The results show that every mineral grain with a size of less than a few  $\mu\text{m}^2$  is encased in a thin carbonaceous matrix, which accounts for only 2.5 wt.%. This interstitial matter sticks together isolated mineral crystallites or concretions, including only very few individualized graphitised grains. Grinding separates the mineral particles but most of them retain their carbonaceous coating. This Raman study complements recent findings deduced from other spatial analyses performed by microprobe laser-desorption laser-ionisation mass spectrometry ( $\mu\text{L}^2\text{MS}$ ), transmission electron microscopy (TEM) and scanning transmission X-ray microscopy (STXM).

© 2004 Elsevier B.V. All rights reserved.

**Keywords:** Murchison meteorite; Carbonaceous matter; Raman imaging

## 1. Introduction

This study deals with the carbonaceous chondrite collected from the Murchison district of Australia in 1969 [1–3]. This meteorite was described as containing 97.5 wt.% mineral: pyroxene (aluminium silicate), enstatite and serpentine (magnesium silicates), olivine (magnesium silicates and iron sulphides) and iron oxides; the remaining 2.5% is composed of carbonaceous matter [2]. Sintered aggregates of olivine and of olivine and pyroxene are described as the most common

objects in chondrites [4,5]. A recent study showed that almost half of the Murchison meteorite consists of fine grained matrix phases dominated by iron sulphides and serpentine, while olivine is the dominant mineral of coarse-grained components [6].

Carbonaceous matter 'on Earth' may include graphite and diverse polyaromatic pre-graphitic materials, like kerogens and solidified bitumens originating from organic matter transformed during complex metamorphic processes [7–11]. Indeed many organic molecules have been detected in Murchison meteorite in ppm amounts: aliphatic and aromatic hydrocarbons [1,12,13], fullerenes [14] and carboxylic acids [1,12]. Biogenic materials like amino acids [3,15,16], puric

\* Corresponding author. Tel.: +33 1 4978 1115; fax: +33 1 4978 1118.  
E-mail address: [marie-helene.baron@glvt-cnrs.fr](mailto:marie-helene.baron@glvt-cnrs.fr) (M.-H. Baron).

nucleic bases [17] and sugars [18] have also been extracted and quantified.

Several works have already been dedicated to the study of the spatial distribution of the carbonaceous matter in chondrites [5,19–22]. Faceted graphene sheets with large-scale graphitisation were found in the Allende meteorite [21] in Fe-rich matrix of olivine especially [22]. Recently non-destructive nuclear reaction analysis (NRA) showed that olivine grains in chondritic meteorites generally have carbon content lower than 120 ppm [5]. Microprobe laser-desorption laser-ionisation mass spectrometry ( $\mu\text{L}^2\text{MS}$ ) [13], isotopic analysis (ion microprobe) and transmission electron microscopy (TEM) [23] and also energy scanning transmission X-ray microscopy (STXM) [24] actually allow reflecting the distribution of different chemical constituents in meteorite samples. The  $\mu\text{L}^2\text{MS}$  method yielded the spatial localization of polycyclic aromatic hydrocarbons in the Allende and Murchison carbonaceous chondrites at approximately 40  $\mu\text{m}$  spatial resolution. While highly selective and very sensitive, this methodology based on desorption is however destructive [13]. TEM analyses enabled following at nano-scale resolution the chemical abundances of titanium carbide in single composite graphite grains of a fragment of the Murchison meteorite [23]. STXM mapping distinguishes domains containing graphite from domains containing amorphous or organic carbon in single chondritic interplanetary dust particles with a spatial resolution of 100 nm [24]. Meaningfully, both TEM and STXM analyses require ultra-microtome slicing of the samples (70–200 nm thick).

Recently Popp et al. demonstrated that point-by-point Raman imaging might provide the distribution of various components, in situ in unpolished chondrites, within surfaces of few  $\mu\text{m}^2$  size [25]. The present Raman study aimed to reveal whether such an imaging method was relevant to map the distribution of minerals in a sample of Murchison chondrite and simultaneously determine the texture of the carbonaceous matter. To our knowledge this is the first time that a Murchison stone has been imaged by means of Raman micro spectrometry. Useful data was obtained on both external and internal domains by scanning the surfaces of native and crushed stone respectively.

The spatial resolution actually available by Raman is coarser than that of TEM and STXM analyses. Moreover, the detection and mapping of a chemical component by Raman has two essential requirements, namely that the sample is relatively dense and/or has a high Raman cross-section. Furthermore, a few ppm or less of bioorganic substances cannot be imaged, excepted if surface-enhanced Raman spectroscopy is available [26,27]. Lastly, the thickness of a molecular layer that can be probed depends —on the indicia of this layer,—on the laser light-absorption by the chemical compounds in the layer and also —on the re-absorption of the light diffused by the probe substances. Despite these limitations Raman has the invaluable advantage of revealing chemical textures of peripheral layers without being destructive.

The present study represents a preliminary analysis enabling to enumerate and size composite domains at micro-metric scale including mineral/carbonaceous interfaces and overlapping materials in the carbonaceous Murchison meteorite. In following up studies other methods should be applied to yield more accurate morphological and chemical details at nanometer scale. The detected complex domains may be those containing the memory of the meteorite formation and its subsequent alteration through the ages. The spatial depiction of molecular interfaces is key for understanding how mineral and organic matter condensed together during solar system formation and possibly before [3,5,19–22,28].

## 2. Experimental

### 2.1. Samples

The studied specimens of Murchison meteorite consisted of several grains measuring  $\sim 2\text{ mm} \times 2\text{ mm}$  each. They were provided by Dr. Michèle Denise (Museum d'Histoire Naturelle, Paris). The specimens were kept in a hermetic box to avoid contamination. Some grains were reduced to a fine powder ( $\sim 1\text{--}5\ \mu\text{m}$ ) in an agate Specamill grinder just before Raman mapping. The equipment (grinder, tubes, balls, etc.) was washed twice with distilled water and ethanol, sonicated for 15 min and autoclaved at 90 °C for 30 min before use. Stones were placed and powders spread on glass plates that had been cleaned with distilled water and ethanol. A cover slip placed over the spread powders prevented them from moving.

### 2.2. Raman microscopy

To test the stability of the samples under green laser beams numerous Raman spectra of native stones or powders were recorded with a Dilor XY Raman spectrometer, equipped with a coherent spectrum Argon ion laser ( $\lambda_{\text{ex}} = 514.5\text{ nm}$ ) and a CCD detector. Using 50 $\times$  objective the laser was focussed onto 4–5  $\mu\text{m}^2$  at the surface of the samples, no matter what it is. The penetration depth of the laser through the black carbonaceous layer should be sub-micronic, as already referred [9]. A spectrum (1) was recorded in focussing the laser (40  $\mu\text{W}$ ) onto an area during 300 s, then another (spectrum 2) in focussing a same power on this area, but during 3000 s. The spectrum of another area irradiated during 3000 s at 40  $\mu\text{W}$  (spectrum 3) was compared to the spectrum of this area subsequently irradiated during 300 s only, but at 400  $\mu\text{W}$  (spectrum 4). A last measure was performed during 3600 s with the laser set at 34  $\mu\text{W}$  and focused on individual areas scanned in time along a line of  $2 \times 80\ \mu\text{m}^2$  size (spectrum 5). Each area along this line was finally only irradiated during 80 s (at 34  $\mu\text{W}$ ). Superimposing spectra 1 and 2 showed that profiles were similar but spectrum 1 ten times weaker than spectrum 2. Spectra 3–5 were nearly identical (intensity). In general, intensities and band-ratio only depended on which

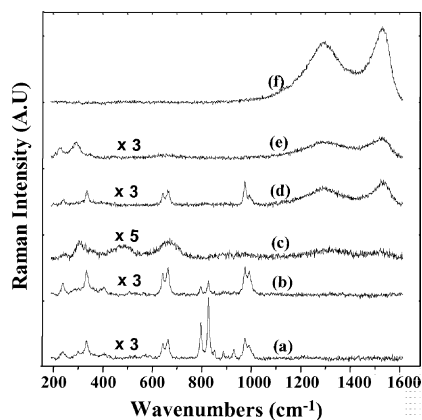


Fig. 1. Representative Raman spectra of areas  $1 \mu\text{m}^2$  at the surface of the specimen of Murchison meteorite used for Raman imaging. Laser focused onto glassy region (a, b) pyroxene (240, 340, 662, 686, 1011, 1030  $\text{cm}^{-1}$ ) and olivine (826, 859, 922, 965  $\text{cm}^{-1}$ ); onto white domains (c) iron oxides ( $\approx 300, 500, 700 \text{cm}^{-1}$ ), (d) pyroxene and carbonaceous matter ( $\approx 1350, 1600 \text{cm}^{-1}$ ), (e) iron oxyhydroxide ( $\text{FeOOH}$ ) ( $\approx 250, 300 \text{cm}^{-1}$ ) and carbonaceous matter; onto a dark domain (f) carbonaceous matter.

meteoritic zone was tested. Spectral profiles look like those recorded with  $50\times$  objective (Olympus) in 300 s with the LabRam Infinity Jobin Yvon-Horiba spectrometer equipped with Nd–Yag laser (600  $\mu\text{W}$  at 532 nm) and a Pelletier cooled CCD camera (Fig. 1). All results ensure that laser heating did not entail time-dependent change. The state of the carbonaceous matter was unchanged after any Raman analysis.

Planar area of native stones were selected among numerous  $10 \times 10 \mu\text{m}^2$  optical images and mapped in using the  $100\times$  objective (Olympus) of the LabRam Infinity spectrometer (600  $\mu\text{W}$  at 532 nm, in moving the sample on an XY stage. Area of  $100 \mu\text{m}^2$  was the largest suitable to perform Raman cartographies. Gaps in planarity prevent mapping of larger surfaces.  $20 \times 20$  spectra were recorded with a resolution of  $\approx 1 \mu\text{m}^2$ , point-by-point with scanning step size of 0.5  $\mu\text{m}$ . Each spectrum was accumulated over a period of 90 s.  $10 \times 10 \mu\text{m}^2$  areas of the crushed material were analysed in following same procedures. Depending on its size an individual particle ( $\varnothing = 1\text{--}5 \mu\text{m}$ ) could be sampled by 2–4 to 50–100 laser strokes, e.g. a  $2 \times 2 \mu\text{m}^2$  particle probed at 16 distinct points.

For the powdered sample a wider area of  $10,000 \mu\text{m}^2$  was also mapped with the  $50\times$  objective (resolution of  $4\text{--}5 \mu\text{m}^2$ ).  $30 \times 30$  spectra were recorded point by point using a scanning step size of 3  $\mu\text{m}$ . A spectrum corresponds to two accumulated spectra recorded during 30 s each. A unique spectrum may be representative from one to two particles if  $\varnothing = 5 \mu\text{m}$ , to four to five particles if  $\varnothing = 1 \mu\text{m}$ . Punctual duplicate spectra performed on mapped areas confirmed that the laser irradiation did not modify the detected substances.

Raman two-dimensional images of the scanned areas were calculated using the LABSPEC-Dilor software. A map is representative of intensity changes in a delimited spectral range assigned to one chemical entity when the sample is moved under the laser beam, step by step. Maps show the distribu-

tion of individual chemical components. In maps presented in Figs. 2 and 3, the darker a zone, the more abundant is the probed compound in this zone.

Spectral intensities (areas) in ranges  $1011\text{--}1130 \text{cm}^{-1}$  and  $825\text{--}857 \text{cm}^{-1}$  were plotted to characterise pyroxene and olivine, respectively [27]. The range  $630\text{--}730 \text{cm}^{-1}$  enables mapping iron oxides [28–30]. According to a highly documented literature, the  $1200\text{--}1700 \text{cm}^{-1}$  range includes the D (disordered) and G (graphitic) bands, representative of clustered carbon in graphenes materials [7–11,31–34]. The D1 band ca.  $1350 \text{cm}^{-1}$  is associated to  $\text{sp}^3$ -bonded carbon motions in amorphous carbonaceous substances or at the periphery of small graphitic grains (from 10 up to 50 nm) in contact with silica. The spectral range  $1540\text{--}1640 \text{cm}^{-1}$  involves the band of pure graphite ( $1581 \text{cm}^{-1}$  for  $\text{sp}^2$ -bonded carbon motions) and two shoulders named D2 and D3 (or D') which assignments are debated [7–11,31–34]. Resonance processes explain high Raman cross-sections and wavenumber variations in changing the energy of the exciting visible laser beam [31–34]. Moreover, it was experienced that the relative contributions of D2 and D3 varied with the orientation of the *c*-axis of graphite grains, with respect to the laser beam [9,11]. Actually, numerous studies show that D1/G or D1/(G + D2 + D3) spectral ratios strongly depend on which carbonaceous specimen is investigated [7–11,34]. Probing micro-domains D1/G decrease may reflect an average reduction of the size of graphite clusters decreasing the number of  $\text{sp}^2$ -bonded carbon (graphitic matter) with respect to interfacial  $\text{sp}^3$  carbons [34]. In other words,  $D_{1230\text{--}1440 \text{cm}^{-1}}/G_{1540\text{--}1640 \text{cm}^{-1}}$  variations measured at the surface of our native and crushed meteorite samples could mean that the size of the graphitised grains varies, also that orientation of the grains are not uniform. Consequently, we emphasise that maps presently deduced from D1/G ratios are crude images differentiating domains including more or less graphitised zones with random orientation, at micrometric scale. A D1/G increase means that local disorder increases (more amorphous carbonaceous matter) while D1/G decrease means that graphitisation is improved. On the other hand, map of pyroxene/D1 ratio evidences organo-mineral composite zones.

The intrinsic noise of the spectra presented in Figs. 2B and 3B, corresponds to 20–30 arbitrary units (A.U.) displayed in white on left vertical scales in Figs. 2C,D and 3C–F. White zones on the maps signify that probed substances are not detectable.

### 3. Results

Fig. 1 displays the spectra of individual areas ( $4\text{--}5 \mu\text{m}^2$ ) at the surface of one native Murchison piece. Wavenumbers and band-profiles on (a) and (b) spectra reveal that the laser excited micro-domains containing olivine and pyroxene (Table 1) [28]. On spectra c and e other bands are assigned to iron oxide and iron oxyhydroxide (Table 1) [29,30]. Marker bands of mineral were always weak and those as-

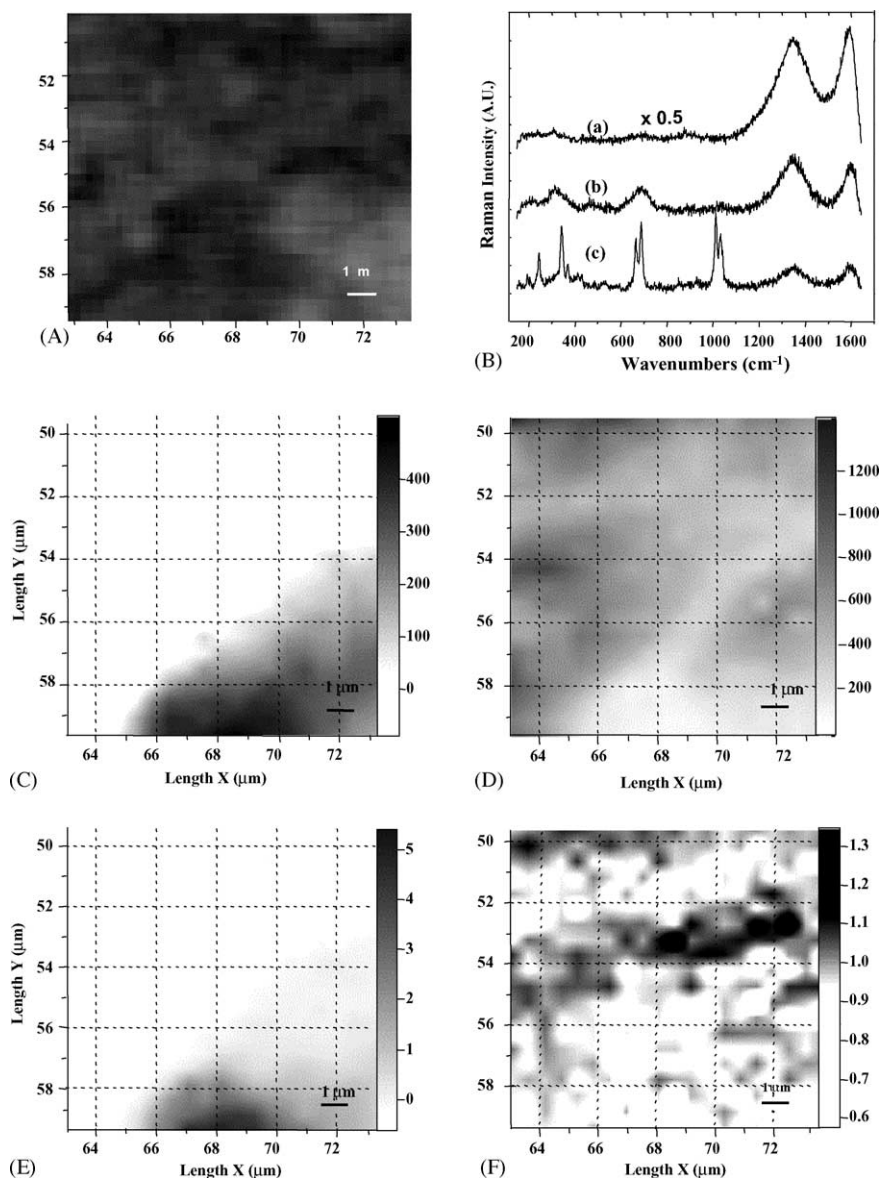


Fig. 2. Two-dimensional distribution of chemical compounds detected in an area of  $100 \mu\text{m}^2$  at the surface of a native Murchison stone. Optical image (A). Punctual Raman spectra (B) with laser focused onto a dark zone (a) carbonaceous matter ( $\approx 1350, 1600 \text{ cm}^{-1}$ ); onto grey zones (b) iron oxides ( $\approx 300, 500, 700 \text{ cm}^{-1}$ ) and (c) pyroxene ( $240, 340, 662, 686, 1011, 1030 \text{ cm}^{-1}$ ) and carbonaceous matter. Raman maps representative of pyroxene (C) ( $1011\text{--}1130 \text{ cm}^{-1}$ ) and amorphous carbonaceous matter (D) ( $1230\text{--}1440 \text{ cm}^{-1}$ ); right axes scale Raman areas in selected wavenumber ranges (A.U.). Raman maps representative of superposed distribution of pyroxene and amorphous carbonaceous material (E) [pyroxene/D1] and of amorphous/graphitised carbonaceous matter (F) [D1/G]; right axes scale these ratios.

Table 1

Characteristic Raman shifts of mineral and carbonaceous chemical components found in the Murchison carbonaceous chondrite

Components	Raman shifts ( $\text{cm}^{-1}$ )	
	Pure components	Murchison
Olivine	826, 859, 922, 965 <sup>a</sup>	826, 859, 922, 965
Pyroxene species	$\approx 200\text{--}400, 670, 1000^a$	240, 340, 662, 686, 1011, 1030
Iron oxyhydroxide (FeOOH)	299, 243 <sup>b</sup>	$\approx 300, 250$
Iron oxides (hematite) <sup>b</sup>	1330, 611, 498, 411, 299, 291, 245, 224	$\approx 300, 500, 700$
Carbonaceous matter	$\approx 1600, \approx 1350^c$	$\approx 1600, \approx 1350$

<sup>a</sup> 28.

<sup>b</sup> 29, 30.

<sup>c</sup> 7–11.

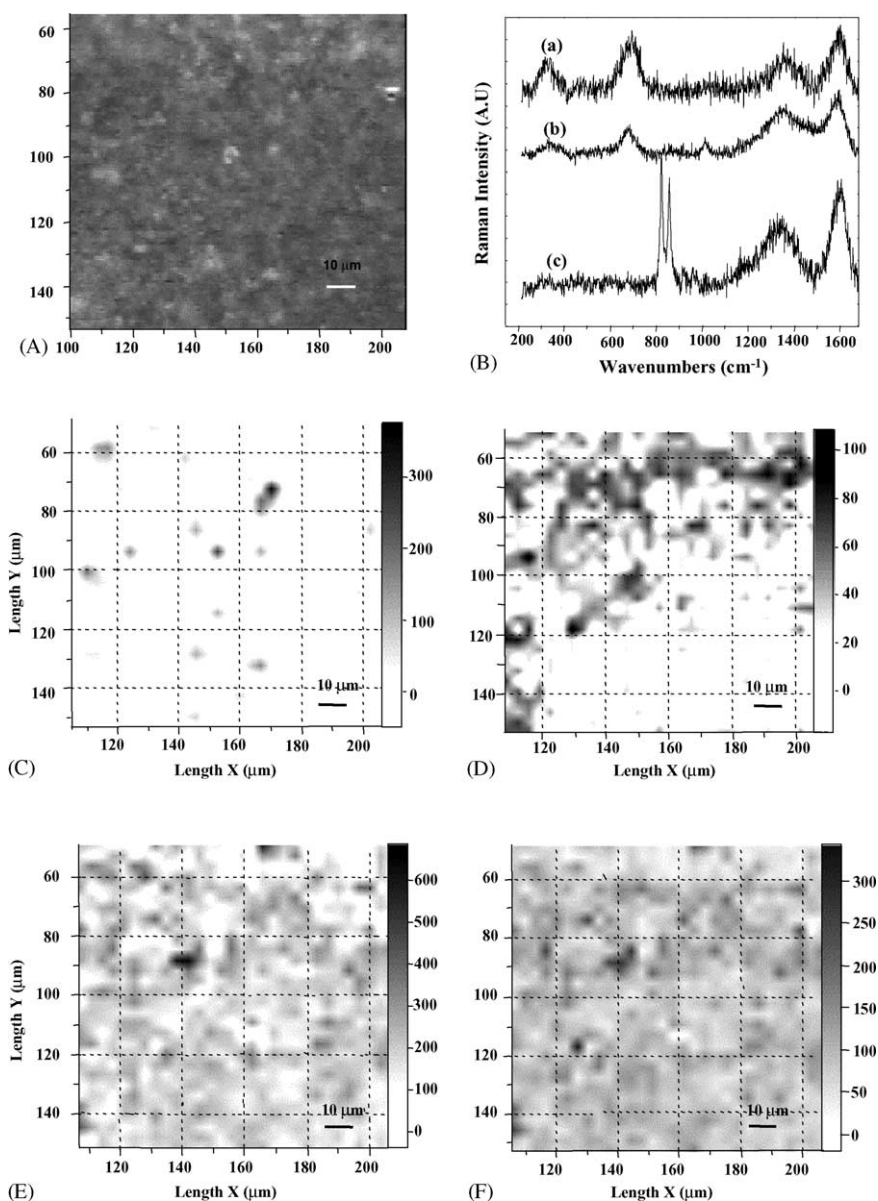


Fig. 3. Two-dimensional distribution of chemical constituents detected in an area of  $10,000 \mu\text{m}^2$  at the surface of crushed Murchison meteorite. Optical image (A). Punctual Raman spectra (B) with laser focused onto dark zones (a, b) iron oxide ( $\approx 300, 500, 700 \text{ cm}^{-1}$ ) and carbonaceous matter ( $\approx 1600, 1350 \text{ cm}^{-1}$ ); onto a white zone (c) olivine ( $825\text{--}857 \text{ cm}^{-1}$ ) and carbonaceous matter. Raman maps representative of olivine (C), iron oxides (D) ( $630\text{--}730 \text{ cm}^{-1}$ ), graphitised (E) ( $1540\text{--}1640 \text{ cm}^{-1}$ ) and amorphous (F) ( $1230\text{--}1440 \text{ cm}^{-1}$ ) carbonaceous materials; right axes scale Raman areas in selected wavenumber ranges (A.U.).

signed to iron oxide specifically broad. Bands D1 and G reflect the presence of more or less disordered carbonaceous matter [7–11,31–34] (Table 1). These bands may be found concomitantly with bands representative of either iron oxide (spectrum c), or pyroxene (spectrum d) or iron oxyhydroxide (spectrum e) bands. However, it has to be underlined that among all punctual tests many only evidenced carbonaceous matter, like spectrum f where G- and D1-peaks are prominent. Slight wavenumber variations at the top of D1 and G peaks as well as changes in line-width indicate that depending on the point probed at the meteorite surface carbon adopts different electronic configurations, as previously found in numerous other geochemical carbonaceous materials [7].

The optical image of an area of  $100 \mu\text{m}^2$  selected at the surface of a native stone is reproduced in Fig. 2A ( $100\times$  objective). The spectra shown in Fig. 2B correspond to different excited points ( $\approx 1 \mu\text{m}^2$ ) selected on this area. Spectra show that the laser might excite pyroxene, iron oxide and carbonaceous matter. Raman maps of the optical image are drafted in Fig. 2C and D. Grey and black zones in map C represent pyroxene. This mineral is directly accessible in a limited area ( $\approx 4 \times 1.5 \mu\text{m}^2$ ). By contrast, the area representative of disordered carbon (amorphous matter) probed by the intensity of the D1-band (grey and dark grey zones in map D) covers most of the analysed surface, except a place exclusively occupied by pyroxene. A comparison of maps C and D indicates that

in the lower-right section, pyroxene and carbonaceous matter overlap. The map representative of pyroxene/D1 reinforces these observations (map E). In the light grey zone, in the lower-right section of the map, pyroxene/D1 ratio increases from 0.5 to 1.5. Little carbonaceous matter seems to be impregnated in the mineral phase at micrometric scale [35]. The map of the most graphitised zones (intensity of the G-band, not shown) was not easily differentiated from that of disordered carbon (map D). However D1/G ratios plotted in map F display a white irregular line pinpointing where graphitisation is more important ( $\approx 2 \mu\text{m}$  in width). Graphitised carbon is also enwrapped in zones where pyroxene and amorphous carbonaceous matter are superimposed.

Similar features were detected on other domains at the surface of the native stone. We conclude that the surface of this stone is mostly made of carbonaceous matter with varying contents (extent) of graphitic and amorphous materials (zones) mixed intimately at micrometric scale, as seen by D1/G ratios oscillating between 0.5 and 1.5. Amorphous carbonaceous, more than graphitised matter partially overlapped pyroxene, scarcely detected.

To better detect the abundant mineral matter (97.5 wt.%) enclosed in carbonaceous Murchison material, crushed samples were analysed. The laser-scanned  $100 \mu\text{m}^2$  areas of a layer of particles (1–5  $\mu\text{m}$  size each) spread over a glass plate (cf. experimental). Surprisingly most of the recorded punctual spectra only revealed D1- and G-bands. Carbonaceous matter was found nearly everywhere over the crushed particles and mineral substances generally indiscernible. Apparently grinding did not affect the state of the carbonaceous matter [9].

The surface of the powder over the glass plate was relatively planar. Thus, it was possible to generate a wider Raman map in expecting to detect more mineral substances. The optical image reported in Fig. 3A represents an area of  $10,000 \mu\text{m}^2$  of meteoritic powder, representative of approximately 500 particles (cf. experimental). At low resolution (4–5  $\mu\text{m}^2$ ) a single laser stroke could excite more than one particle (4–5 particles for smallest). Punctual spectra revealed the presence of three species: olivine, iron oxides and carbonaceous matter (Fig. 3B). The  $10,000 \mu\text{m}^2$  maps are shown in Fig. 3C–F. Olivine appears in discrete domains 2–3  $\mu\text{m}$  across (map C). The zones over which iron oxide is visible are more diffuse (grey-black zones on map D). These domains may represent randomly superposed iron rich flat grains of a few microns each. The comparison of maps C and D indicates that each olivine spot stands in a zone where iron oxide concretions are not detected (grey spots on map C/olivine coincide with white zones on map D/iron oxide). In map C, except the single black spot, other light-grey spots correspond to grey areas on maps E and F. This means that carbonaceous matter covers most of the detected olivine spots. In many regions where iron oxide is dense (dark-grey zones in map D) carbonaceous matter is also present (grey zones in map F) but not well graphitised (white zones in map E). Besides, where disordered carbon reaches highest levels, graphitised

carbon reaches high levels too (see dark-grey and black zones at same places in maps E and F. A delimited black spot is exactly at the same place in maps E and F. It might correspond to a graphitic spherule ( $\varnothing \approx 3\text{--}4 \mu\text{m}$ ) [23].

#### 4. Discussion

Green lasers focussed onto Murchison meteoritic samples with mm or  $\mu\text{m}$  thickness (stones or powders, respectively) did not generate any heating alteration [9]. This was evidenced when controlling intensities and profiles of the Raman bands over periods of 3600 s for the longest, with powers ranging between 34 and 600  $\mu\text{W}$  and  $50\times$  and  $100\times$  objectives.

Carbonaceous matter was detected nearly everywhere over the surface of our native meteoritic pieces. Only micrometric asperities of pyroxene, partly invaded by carbonaceous clusters were detected. Because the laser beam only probes the black envelope at sub-micrometer depths most of the mineral matter is hidden [9,34]. This explains why olivine, which is the major component of the meteorite, was not detected when mapping the surface of the native stone [4,6].

De facto, more olivine and iron oxides were statistically detected at the surface of the powdered sample ( $10,000 \mu\text{m}^2$ ) than at the surface of native pieces ( $100 \mu\text{m}^2$ ). However surprisingly, mineral species were still hard to detect, taking into account of the spatial resolution used.

How can such a low percentage of carbon quantified in the chondrite (2.5 wt.%) gives rise to such highly extended carbonaceous surfaces and as great at the surface of the powder as at the surface of a native stone? The only pertinent answer found is that our crushing procedure did not cleave any mineral micro crystallite or concretion and that after crushing a thin black film still screened most of them from the green laser light. Crushing might have only thoroughly divided the studied stones ( $\approx 2 \text{mm} \times 2 \text{mm}$ ) into micrometric particles (1–5  $\mu\text{m}$ ) but not removed carbonaceous coating around the mineral grains. Only sporadically where coating is thin enough the laser excites olivine matter. This is consistent with the fact that carbonaceous matter surrounds most of the detected olivine spots. This is also true for oxide iron-rich particles, but because they were detected more easily than olivine, a thinner carbonaceous film should wrap them. Mapping of the crushed sample allows the discrimination of olivine- and iron oxide-rich particles. Whether or not individual grains were disjointed during crushing, each olivine crystallite or iron oxide concretion seems to be isolated from each other by a layer of carbonaceous matter. More than forming local dense inclusions, the carbonaceous matter impregnates a dense phase of individual mineral grains, each of micrometer size [4,5,24,36,37]. The strong cohesion of the original specimens could be due to the great stickiness of a three-dimensional organic network. While representing only 2.5 wt.% of the native rock, the carbonaceous material

appears to hold together a tremendous number of tiny mineral crystallites and concretions (97.5 wt.%).

On Earth, organic matter adsorbs on minerals [27]. This may favour redox reactions destroying part of the organic matter (oxidation) but transforming another part (reduction) into kerogenous material stocked onto the minerals. Next, either orientated pressures and elevated temperatures, or high temperatures only and contact with magma, may entail graphitisation [11]. The Murchison chondrite landed on Earth in 1969 [2]. Because pre-graphitised carbon seems to enwrap all mineral concretions standing at the surface of the stone, but also deep inside, most of the carbonaceous metamorphism should have happened before mineral grains aggregation, thus not on Earth after landing, neither in Earth atmosphere before landing.

Ion irradiation of frozen organic compounds, similar to those found in ppm amounts in the meteorite [1,12,13], was recently performed to mimic the exposition of interplanetary dusts (IDPs) to solar wind particle flux and fast solar proton ion flux. The Raman D–G Raman features of the resulting samples do not exactly fit with the features recorded for IDPs [36]. Other parameters have to be added to reproduce carbonaceous states in IDPs and meteorites. Solar or interstellar mineral dusts (~400 μm) are made of iron-rich olivine materials [1,3,24,37–40]. Metal oxide could have favoured the adsorption of solar or interstellar organic molecules and catalysed specific photo-redox processes delivering volatile entities (oxidized) but also maintaining amorphous reduced organic material onto the dusts. The stickiness of such peripheral carbonaceous layer could have favoured the capture of bare dusts (pyroxene and olivine) to form heterogeneous concretions onto which other sticky dusts could have been fixed, and so on repetitively, implementing through ages the meteorite size. This could explain why carbonaceous matter in IDPs, always submitted to ion-irradiation, is in average slightly different from meteoritic carbonaceous matter protected from ion radiation after dust aggregation [36].

## 5. Conclusion

Micro Raman spectroscopy is one of the best tools to perform rapid and non-destructive analyses of carbonaceous matter at the surface of meteorites and fossils [25,41,42]. A series of missions to Mars is planned which will include in situ analyses and collection of samples suitable for transporting them to Earth. The present results support the idea that a rover-based Raman spectrometer on Mars surface could provide good initial data on carbonaceous matter distribution. This may help in the selection of appropriate micro samples to be brought back to Earth for further investigations [43,44].

## Acknowledgements

The CNRS, the University of Paris VI (France), the Centre National d'Études Spatiales (CNES) and the French Exobi-

ology GDR supported this work. C. El Amri holds a post-doctoral fellowship from the CNES. We thank Richard Mandel for manuscript improvement.

## References

- [1] O. Botta, J.L. Bada, *Surv. Geophys.* 23 (2002) 411.
- [2] L.H. Fuchs, E. Olsen, K.J. Jensen, *Mineralogy, mineral-chemistry and composition of the Murchison (C2) meteorite*, *Smithson. Contrib. Earth Sci.* 10 (1973) p. 39.
- [3] P. Ehrenfreund, S.B. Charnley, *Earth Ann. Rev. Astron. Astrophys.* 38 (2000) 427.
- [4] J.L. Gooding, K. Keil, *Meteoritics* 16 (1980) 17.
- [5] M.E. Varela, N. Metrich, *Geochim. Cosmochim. Acta* 64 (2000) 3433.
- [6] S. Pizzarello, M.E. Zolensky, K.A. Turk, *Geochim. Cosmochim. Acta* 67 (2003) 1589.
- [7] B. Wopenka, J.D. Pasteris, *Am. Mineralogist* 78 (1993) 533.
- [8] F. Tuinstra, J.L. Koenig, *J. Chem. Phys.* 53 (1970) 1126.
- [9] O. Beyssac, B. Goffe, J.P. Petit, E. Froigneux, M. Moreau, J.N. Rouzaud, *Spectrochim. Acta A* 59 (2003) 2267.
- [10] O. Urban, J. Jehlicka, J. Pokorny, J.N. Rouzaud, *Spectrochim. Acta A* 59 (2003) 2331.
- [11] J. Jehlicka, O. Urban, J. Pokorny, *Spectrochim. Acta A* 59 (2003) 2341.
- [12] J.R. Cronin, S. Chang, et al., *Organic matter in meteorites: molecular and isotopic analyses of Murchison meteorite*, in: J.M. Greenberg (Ed.), *Chemistry of Life's Origin (NATO ASI)*, Kluwer, Dordrecht, 1993, pp. 209–258.
- [13] F.L. Plows, J.E. Elsil, R.N. Zare, P.R. Buseck, *Geochim. Cosmochim. Acta* 67 (2003) 1429.
- [14] L. Becker, R.J. Poreda, T.E. Bunch, *Proc. Natl. Acad. Sci.* 97 (2000) 2979.
- [15] S. Pizzarello, J.R. Cronin, *Nature* 394 (1998) 236.
- [16] J.R. Cronin, G.W. Cooper, S. Pizzarello, *Adv. Space Res.* 15 (1995) 91.
- [17] P.G. Stoks, W. Schwartz, *Geochim. Cosmochim. Acta* 46 (1982) 309.
- [18] G. Cooper, N. Kimmich, W. Beliste, J. Sarianana, K. Brabham, L. Garrel, *Nature* 414 (2001) 879.
- [19] J. Makjanic, R.D. Vis, W.J. Hovenier, D. Heymann, *Meteoritics* 28 (1993) 63.
- [20] P. Hanon, F. Robert, M. Chaussidon, *Geochim. Cosmochim. Acta* 62 (1998) 903.
- [21] P.J.F. Harris, R.D. Vis, D. Heymann, *Earth Planetary Sci. Lett.* 183 (2000) 355.
- [22] A. Brearley, *Science* 285 (1999) 1380.
- [23] T.K. Croat, T. Bernatowicz, S. Amari, S. Messenger, F.J. Stadermann, *Geochim. Cosmochim. Acta* 67 (2003) 4705.
- [24] G.J. Flynn, L.P. Keller, C. Jacobsen, S. Wirick, *Adv. Space Res.* 33 (2004) 57.
- [25] J. Popp, N. Tarcea, W. Kiefer, M. Hilchenbach, N. Thomas, S. Hofer, T. Stuffer, S.S. Hoffer, D. Töffer, A. Greshake, *Planet Space Sci.* 50 (2002) 865.
- [26] C. El Amri, M.H. Baron, M.C. Maurel, *J. Raman Spectrosc.* 35 (2004) 170.
- [27] C. El Amri, M.H. Baron, M.C. Maurel, *Spectrochim. Acta A* 59 (2003) 2645.
- [28] A. Wang, B.L. Jolliff, L.A. Haskin, *J. Geophys. Res.* 104 (1999) 8509.
- [29] D.L.A. De Faria, S. Venacio Silva, M.T. de Oliveira, *J. Raman Spectrosc.* 28 (1997) 873.
- [30] M. Bouchard, D.C. Smith, *Spectrochim. Acta A* 59 (2003) 2247.
- [31] M. Ramsteiner, J. Wagner, *Appl. Phys. Lett. B* 51 (1987) 1355.
- [32] I. Poscsik, M. Hundhausen, M. Koos, L. Ley, *J. Non-Cryst. Solids* 227–230 (1998) 1083.

- [33] M.J. Matthews, M.A. Pimenta, G. Dresselhaus, M.S. Dresselhaus, M. Endo, *Phys. Rev. B* 59 (1999) 6585.
- [34] P. Colomban, G. Gouadec, L. Mazerolles, *Mater. Corr.* 53 (2002) 306.
- [35] P.D.A. Pudney, T.M. Hancewicz, D.G. Cunningham, M.C. Brown, *Vib. Spectro.* 34 (2004) 123.
- [36] G.A. Baretta, V. Mennella, J.R. Brucato, L. Colangeli, G. Leto, M.E. Palumbo, G. Strazzulla, *J. Raman Spectrosc.* 35 (2004) 487.
- [37] S. Amari, E. Anders, A. Virag, E. Zinner, *Nature* 345 (1990) 238.
- [38] S. Messenger, L. Keller, F.J. Stadermann, R.M. Walker, E. Zinner, *Science* 300 (2003) 105.
- [39] A. Wang, L.A. Haskin, E. Cortez, *Appl. Spectrosc.* 52 (1998) 477.
- [40] E. Zinner, S. Amari, R. Guinness, A. Nguyen, F.J. Stadermann, R.M. Walker, R.S. Lewis, *Geochim. Cosmochim. Acta* 67 (2003) 5083.
- [41] J.W. Schopf, A.B. Kudryavtsev, D.G. Agresti, T.J. Wdowiak, A.D. Czaja, *Nature* 416 (2002) 73.
- [42] H.G.M. Edwards, E.M. Newton, D.L. Dickensheets, D.D. Wynn-Williams, *Spectrochim. Acta A* 59 (2003) 2277.
- [43] A. Ellery, D. Wynn-Williams, J. Parnell, H.G.M. Edwards, D. Dickensheets, *J. Raman Spectrosc.* 35 (2004) 411.
- [44] S.K. Sharma, P.G. Lucey, M. Ghosh, H.W. Hubble, K.A. Horton, *Spectrochim. Acta A* 59 (2003) 2407.